Received: 19 July 2022 | Revised: 20 October 2022 | Accepted: 21 October 2022

DOI: 10.1002/pip.3650

SPECIAL ISSUE ARTICLE

PROGRESS IN PHOTOVOLTAICS WILEY

Autonomous measurement system for photovoltaic and radiometer soiling losses

Laura Campos[1] | Stefan Wilbert[1] | José Carballo[2] | Juliane Meyer zu Köcker[1] | Fabian Wolfertstetter[1] | José La Casa[1] | Erik Borg[3] | Karsten Schmidt[4] | Luis F. Zarzalejo[5] | Aránzazu Fernández-García[2] | Fernanda Norde Santos[1] | Ginés García[2]

[1]DLR Institute of Solar Research, Paseo de Almería 73, 04001, Almería

[2]CIEMAT Plataforma Solar de Almería, Ctra. de Senés s/n km 4, 04200, Tabernas, Spain

[3]DLR Remote Sensing Data Center, Kalkhorstweg 53, 17235, Neustrelitz, Germany

[4]DLR Institute of Remote Sensing Technology, Kalkhorstweg 53, 17235, Neustrelitz, Germany

[5]CIEMAT Renewable Energy Division, Avda. Complutense 40, 28040, Madrid, Spain

Correspondence
Stefan Wilbert, DLR Institute of Solar Research, Paseo de Almería 73, 04001 Almería, Spain.
Email: stefan.wilbert@dlr.de

Funding information
This research was funded by Deutsches Zentrum für Luft- und Raumfahrt (DLR) and Centro de Investigaciones Energéticas, Medioambientales y Tecnológicas (CIEMAT).

Abstract

Soiling can greatly reduce both the efficiency of photovoltaic (PV) installations and the signals of radiometers. The knowledge of the current soiling losses of a PV installation can be used to optimize the cleaning schedule and to avoid false alarms related to other issues that might cause underperformance. Underperformance can be detected by comparing measured to modeled PV production derived using pyranometer or reference cell measurements. Soiled pyranometers or reference cells lead to too low modeled PV production so that PV soiling or other errors might not be detected. So far, soiling sensors either require frequent cleaning or they use indirect measurements to derive the soiling loss (e.g., analysis of backscattering signal or imaging of dust on a glass surface). Currently, the soiling loss of pyranometers or outdoor reference cells uses the comparison to another frequently cleaned device of the same model. To avoid time-consuming maintenance of the sensors and to avoid additional sensors as much as possible, we developed a new method for measuring PV and radiometer soiling losses. The method makes use of a characterized lamp that is protected from soiling by a collimator and that illuminates the pyranometer or reference cell each night for some time. Comparing the signals of one night to the signal obtained at a night shortly after the last cleaning of the sensor, its soiling loss can be derived. To validate the measurements of soiling losses for the pyranometer and the reference cell, the soiling losses of the devices are also derived by comparing their signals to those of a clean sensor of the same type. These reference instruments are calibrated relative to the test devices so that deviations indicate the soiling loss of the test sensors. The first outdoor tests with 4 months of data show a good agreement with the reference measurements of the soiling losses. The accuracy of the method is estimated to be similar to that of the reference method, which involves the daily cleaning of the reference devices.

KEYWORDS
irradiance measurement, pyranometer, reference cell, soiling

1 | INTRODUCTION, AIM, AND APPROACH

Soiling can greatly reduce both the efficiency of photovoltaic (PV) installations and the signals of radiometers. In the case of PV systems, it has been estimated that soiling reduces the global power production by 3% to 4%.[1] For radiometers such as pyranometers that are used to measure global horizontal irradiance (GHI) or global tilted irradiance (GTI), several studies investigated the signal reduction[2,3] and have shown that soiling can cause relevant uncertainty contributions.[4] The knowledge of the current soiling losses of a PV installation can be used to optimize the cleaning schedule[5] and to avoid false alarms related to other issues that might cause underperformance.[6] Underperformance can be detected by comparing measured to modeled PV production derived using pyranometer or reference cell measurements. Soiled pyranometers or reference cells lead to too low modeled PV production so that PV soiling or other errors might not be detected.

Several PV soiling sensors are available to measure the related losses at one or more sites in the PV installation. Pairs of clean and soiled, but otherwise identical PV reference cells[7] or modules[8] can be used to derive the soiling loss by comparing their power or short-circuit current. Such sensors either require stable radiation conditions and frequent cleaning of one of the two devices. Automatic and even manual cleaning can be incomplete and result in measurement errors. On days with mostly overcast or highly variable conditions, deriving the soiling loss is complex and connected to higher uncertainties compared to sunny conditions.

Other sensors use indirect measurements to derive the soiling loss (e.g., analysis of scattering signal[9] or imaging of dust[10]). The scattering type sensor (Dust IQ) uses a pulsed LED in a weather proof case beneath a glass cover that is exposed to soiling in the plane of the PV modules. A photodiode in the same case measures the LED radiation scattered towards back in the enclosure. The scattering signal increases due to soiling of the outer surface of the glass cover. A calibration of the scattering signal allows to convert the photodiode signal to the soiling loss. This calibration can be done on site using two PV cells mounted in the same device with the same cover glass. The cover glass above the two PV cells are cleaned one after the other during stable sunny conditions at low incidence angles and it is assumed that the glass surface of the device is soiled homogeneously.

The MARS sensor takes images of the particles on a glass surface equipped with black and white reference marks from within a weather proof enclosure. Pictures taken using the sun as light source reveal particles attenuating the incoming radiation, so that the average brightness of the image is related to the soiling loss. Next to the camera, LEDs are placed that can illuminate the dust particles from the inside of the enclosure. Images taken at night with the LEDs as light source appear brighter if dust particles are on the glass surface due to the backscattered light. This information is used to correct the attenuation information obtained with the sun as a light source. These sensors are interesting because of the low maintenance effort but have also shown to be less accurate than pairs of soiled and cleaned PV devices in a comparison of soiling sensors.[11]

To avoid time-consuming maintenance of the sensors and to avoid additional sensors as much as possible we developed a new method for measuring PV and radiometer soiling losses. The method uses a lamp that illuminates a pyranometer or PV reference cell for about 45 min at night. By comparing the irradiance measured at night with that of another night when the sensor was clean, the soiling loss can be derived. Several 45 min long measurements are combined to detect erroneous soiling measurements caused by dew, rain droplets on the radiometer, or other effects that might only be present in some of the various measurements. We refer to this new method as "Radguard."

This work presents the first method of measuring soiling of already installed PV reference cells or pyranometers without adding another similar radiometer that is frequently cleaned. If a reference cell is already installed the method allows to include a soiling measurement to a PV plant with an inexpensive lamp system is and only adds the lamp temperature measurement to the data acquisition system. The Radguard method is based on the work of Borg et al.[12] and has similarities to the independently developed approach from previous studies.[13–15] This other setup is called DUSST and also uses a LED light source to illuminate a soiled sensor or a glass beneath which a light detector is placed. The DUSST system's lamp is directly attached to its radiation sensor, and the evaluation requires a measurement and control unit. A general difference is that Radguard can be used for different radiometers including pyranometers. Soiling losses of pyranometers or reference cells that are already installed cannot be measured with the DUSST. If a reference cell is already used in the PV plant, the PV soiling measurement can be obtained with Radguard by adding only the lamp depending on the existing data logger and power supply, thus potentially saving investment costs compared to the DUSST. The Radguard lamp might be connected to an existing power supply and datalogger if the logger also allows to switch on certain power connections from time to time and if it has a free channel for a PT100. If the logger cannot control the lamp power connection, an inexpensive time controller is needed that is programmed once before the installation. The evaluation of the Radguard signal can be done based on the nightly irradiance measurements of the radiometer that can be

logged by a previously existing data logger. Also, the Radguard setup uses longer distances between the radiometer and the light source. This allows a long collimator that efficiently protects the light source from soiling. Furthermore, the Radguard lamp is installed such that it does not affect the radiation measurements taken by the radiometer, which is not foreseen with the DUSST system. Thus, a reference cell or pyranometer with a Radguard lamp serves for both the radiation and the soiling measurement. Note that frequent sensor cleaning is recommendable to ensure the highest possible accuracy. If daily cleaning is used, Radguard will only detect noticeable soiling losses in extreme cases (e.g., sandstorm). If only weekly cleaning is used, as recommended for accuracy class A PV monitoring in IEC 61724-1, Radguard will be able to detect soiling more often. In this case, the combination of the lamp and radiometer measures both irradiance and soiling loss. For less frequent cleaning intervals, the irradiance measurement accuracy will be reduced. The maximum duration between two cleaning events is also limited by the stability of the lamp. This stability is briefly discussed in the conclusion.

Another difference is that the DUSST sensor uses short light pulses to avoid a temperature increase of the lamp so that its temperature is estimated using the ambient temperature. In Radguard, the lamp temperature is measured directly with a PT100 temperature sensor installed next to the LED light.

In Section 2, we describe the new soiling measurement method in more detail before the characterization of the lamp is presented in Section 3. Section 4 explains the performed outdoor test of the soiling measurement system. In Section 5, the results of the system validation are discussed. Finally, the conclusion and an outlook are presented.

2 | DESCRIPTION OF THE SOILING MEASUREMENT METHOD

The setups for the soiling measurement of pyranometers and PV are shown in Figure 1. The lamp is installed on one end of a 90° angle structure. On the other side of the structure is the corresponding sensor, a pyranometer or a reference cell.

The lamp, shown in Figure 2, is a RS2600 pocket light, to which a PT100 temperature sensor was attached close to the LED. The batteries of the lamp are replaced by a power supply (Meanwell LCM-25 constant current source) that is controlled with a common time controller that switches on the lamp during one or more 45 min intervals at night.

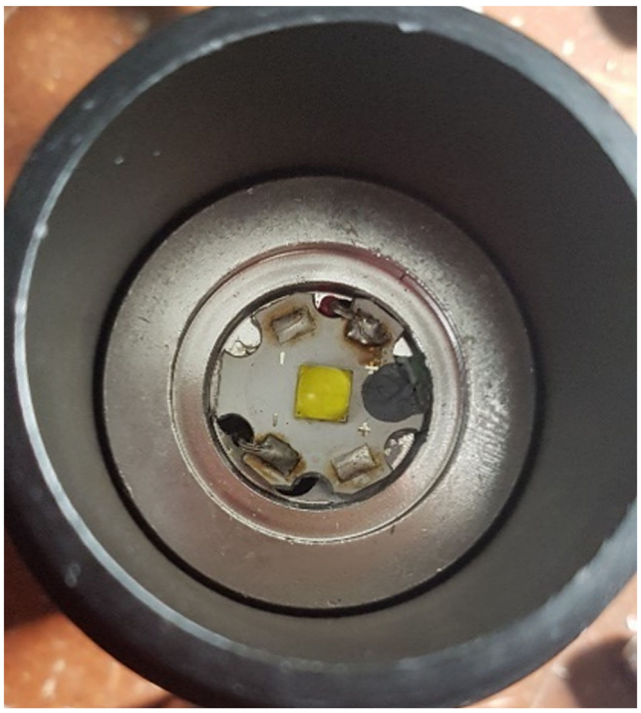

FIGURE 2 LED, connections, and PT100 temperature sensor (covered with thermo-paste) [Colour figure can be viewed at wileyonlinelibrary.com]

FIGURE 1 Soiling loss measurement systems for a pyranometer installed on a fixed structure (left) and for a reference cell/PV (right) [Colour figure can be viewed at wileyonlinelibrary.com]

The lamp is protected against soiling by a 25-cm-long conical collimator tube. The collimators outer aperture is open. The conical shape allows for a small aperture that limits the amount of dust entering the collimator to a minimum and also reduces the influence of the collimator on the radiation measurement as less diffuse radiation is prevented from reaching the sensor. The collimator is essential for the method, as the lamp must be protected against soiling.

The fixed position of the lamp is of utmost importance. Therefore, the mechanical setup was selected such, that even small movements are highly unlikely. This is of particular importance if the Radguard setup is installed on a moving platform as a solar tracker or a PV tracker. The mechanical connection is hence done using self-locking nuts.

The structure and the lamp block only a small fraction of the diffuse or ground-reflected irradiance so that the signal of the radiation sensor is not noticeably affected. The angle of incidence (AOI) of the lamp's light for the pyranometer setup is 45° and for the reference cell that is mounted at 30° tilt it is 60°. The incidence angles are selected as a tradeoff between a high irradiance measurement caused by the lamp on the one hand and a low influence on the irradiance measurement on the other hand. For the reference cell setup, the geometry was also selected to avoid any shading of the PV modules.

The data acquisition of the reference cell's short-circuit current and the pyranometer's voltage is done using a Campbell CR1000 datalogger, which can also perform the evaluation of the nightly signals and the calculation of the soiling loss. However, also simpler data loggers and the existing data acquisition system of already installed sensors can be used if the calculation of the soiling signal is done as a post-processing on a separate computer. The latter option was followed in this work. The pyranometer was a CM11. The reference cell is a NES SOZ-03 with textured cover glass.

The irradiance and lamp temperature measurements of one night, close to the time of the illumination, are shown in Figure 3 for an exemplary night and the pyranometer. The illumination interval is visible as a nearly step-like irradiance. The temperature of the lamp rises during the first minutes of the illumination and falls after the lamp is switched off. As the temperature of the lamp affects its emittance, the rise of the temperature at the beginning of the illumination interval causes also changes in the irradiance. Therefore, the irradiance $I_{raw,1min}$ is obtained from the interval in the last minutes before switching off the lamp. The lamp's temperature T_{LED} for the evaluation is also obtained for the same time interval. The remaining variation of the temperature and irradiance is caused by the variation of the wind speed and ambient temperature, as our analysis and laboratory tests showed. Due to the zero offset of the pyranometer, negative irradiances O_1 and O_2 are measured before and after the illumination. These offsets are also included in the calculation of the soiling loss. For the reference cells, the values characterize potential external light sources.

With the four variables, the soiling loss is derived. First, the temperature and offset corrected irradiance $I_{cor,1min}$ of a 1-min average is calculated.

$$I_{cor,1min} = \left(I_{raw,1min} - \frac{O_1 + O_2}{2}\right) \cdot C(T_{LED}). \quad (1)$$

For the calculation, also the temperature correction function C is applied. This function has been derived by evaluating the irradiance measurement of the setup in a climate chamber at various ambient temperatures, as shown in the next section. $C(T_{LED})$ corrects the signal such that $I_{cor,1min}$ corresponds to the irradiance that would be obtained at a lamp temperature of 25°C.

The last 15 min of each illumination interval are evaluated, and the average I_{cor} of the 15 $I_{cor,1min}$ values is calculated. Comparing I_{cor} of a night for which the soiling loss should be derived with $I_{cor,clean}$, measured during the night after the last cleaning event, the soiling loss S can be calculated at the time at which I_{cor} is measured.

$$S = 1 - \frac{I_{cor}}{I_{cor,clean}}. \quad (2)$$

To automatically detect the parameters required for the calculation of the soiling loss, the illumination intervals are detected as time stamps at night for which the irradiance exceeded a certain threshold. For the pyranometers, 50 W/m^2 is used as threshold and for the reference cell 25 W/m^2. The threshold for the reference cell is lower due to the lower signal caused by the AOI (60° instead of 45° for the pyranometer) and the lamp properties. O_1 is the average of the irradiance 30 min just before the illumination and O_2 of 30 min after the illumination.

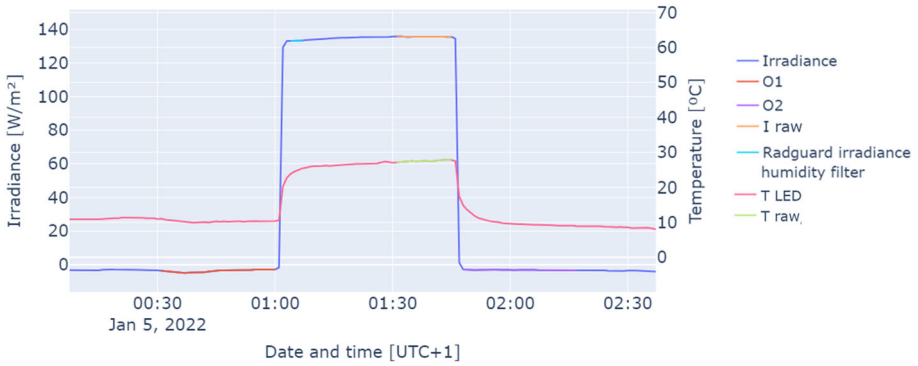

FIGURE 3 Irradiance and lamp temperature measurements in the night of 5 January 2022 close to the time of the illumination for a pyranometer. [Colour figure can be viewed at wileyonlinelibrary.com]

2.1 | Incidence angle correction for the reference cell setup

To derive the PV soiling loss data given moment in time, the data from the Radguard system have to be corrected for AOI effects. As the lamp is measuring at an AOI of 60°, the soiling loss obtained with Equation 2 is expected to be higher than that, for example, at solar noon where lower incidence angles are typically found and which is more characteristic for the average daily soiling losses. This AOI effect has been described in the literature (e.g., previous studies[16–18]). The soiling losses increase with AOI up to about 80° as the optical path through the soiling layer increases with the AOI. For even higher AOI the soiling loss decreases and even higher irradiances or PV power are found due to scattering gains. For the pyranometer an incidence angle correction is not applied as the geometry of the dome avoids an AOI effect.

The AOI effect and corrections for it were studied for the specific reference cells used here by Wolfertstetter et al.[7] For sunny conditions with a large contribution of direct irradiance to GTI correction factors for the soiling ratio were reported for AOIs between 0° and 70° as a function of the soiling ratio at 34° AOI. The soiling ratio is the ratio of the signal with a given soiling loss to the signal expected for a clean device. The reported correction factors depend on the soiling ratios. The correction factors for soiling ratios of 0.9925 and 0.9625 (both at 34° AOI) from Wolfertstetter et al.[7] are used and a linear dependence of the correction factor on the soiling ratio is assumed. As the average AOI used to determine the reference data to which the Radguard results are compared in Section 5 is about 28°, we derive the correction to this specific AOI. This leads to the following AOI correction in terms of the soiling loss S (here in percent), for soiling losses $S(60^\circ)$ above 0.5%.

$$c_{AOI} = \left(1 - \frac{S(60^\circ)}{100}\right) \cdot (-0.3199) + 1.322, \tag{3}$$

$$S(28^\circ) = \left(1 - \left(1 - \frac{S(60^\circ)}{100}\right) \cdot c_{AOI}\right) \cdot 100. \tag{4}$$

The corrections are modified for soiling losses at AOI of 60° below 0.5% in order to avoid that soiling gains at 28° AOI are obtained and to guarantee a monotonically increasing correction. Therefore, the correction factor is linearly interpolated between 1 at 0 soiling to the results from Equation 3 at 0.5% soiling loss at AOI of 60°. The resulting correction and the relation of the two soiling losses are shown in Figure 4.

3 | CHARACTERIZATION OF THE LAMP

Five lamps were studied to understand the temperature effect on the output irradiance. For this experiment, a Vötsch-ATLAS SC340_MH climate chamber, shown in Figure 5, was used. This chamber allows temperature tests from −40°C to +120°C. The same structure as for the already installed system was mounted inside the chamber, combined with a CMP21 pyranometer to measure the irradiance and the lamp temperature. To avoid reflection, the chamber was covered inside with black foil. The climate chamber was programmed to increase the ambient temperature, every 110 min by 5°C. Starting

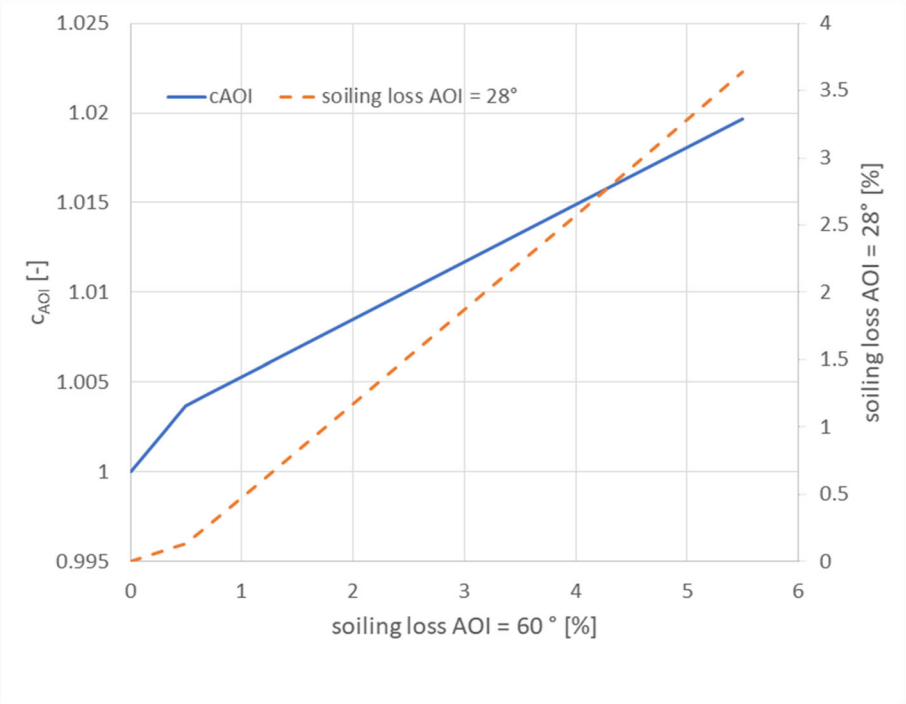

FIGURE 4 Visualization of the AOI correction from Equations 3 and 4 and its effect [Colour figure can be viewed at wileyonlinelibrary.com]

with −10°C, the ambient temperature was increased in 11 steps until 40°C. In the first 55 min, the lamp adjusted to the ambient temperature while in the second 55 min the lamp was switched on by an automatic clock. The illumination interval of 55 min was used to ensure the achievement of a stable lamp temperature. Based on the results from the climate chamber, 45 min illumination intervals were selected for the outdoor tests. During the whole test, the data for the irradiance, lamp temperature, and ambient temperature was collected by a CR1000 datalogger.

FIGURE 5 Setup for testing the temperature dependence of the lamps in a Vötsch-ATLAS SC340_MH climate chamber [Colour figure can be viewed at wileyonlinelibrary.com]

Figure 6 shows the irradiance, the temperature in the climate chamber, and the lamp temperature as a function of the time. The lamp temperature rises and then stabilizes during the illumination intervals. Especially during lower ambient temperature, the irradiance appears stable within one illumination interval. The stability of the lamp's irradiance is reached after a longer stabilization time for higher ambient temperatures.

In the first step for the calculation of the temperature correction, polynomials of degree three are fitted to the irradiance data as a function of the lamp temperature. Only the data when the lamp was switched on and the lamp temperature was stable was taken. The intervals with stable lamp temperature were selected by using only data with a change of less than 0.02°C per minute for most lamps. For lamps SN00 and SN01, the limit was 0.2°C as these lamps include different LEDs and as they were used at higher temperatures and irradiances. The results are shown in Figure 7.

To obtain the temperature correction functions $C(T)$, lamp-specific polynomials were normalized such that their value is 1 at 25°C. The correction functions $C(T)$ for five lamps are shown in Figure 8. The temperature correction varies from lamp to lamp. While some lamps, such as lamp SN03, show only a small temperature dependence that could be neglected, for other lamps, like the lamps SN01 or SN02, the temperature correction is stronger and reaches about 2.5% at a temperature change of 50 K. Therefore, with the currently selected lamps, tests need to be carried out with every individual lamp to characterize the single lamps and calculate a lamp-specific polynomial.

4 | OUTDOOR TEST OF THE SOILING MEASUREMENT SYSTEM

The test and reference devices have been operated for several months and a comparison of the acquired data has been performed. For the pyranometer, data from 27 December 2021 until 14 March 2022 and for the reference cell data from 18 May 2022 until 28 June

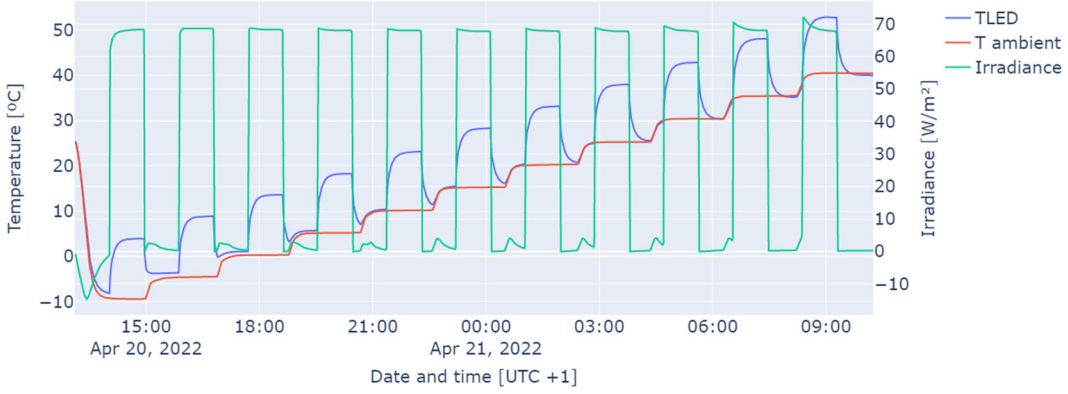

FIGURE 6 Irradiance and temperature measurements of one lamp in the climate chamber [Colour figure can be viewed at wileyonlinelibrary.com]

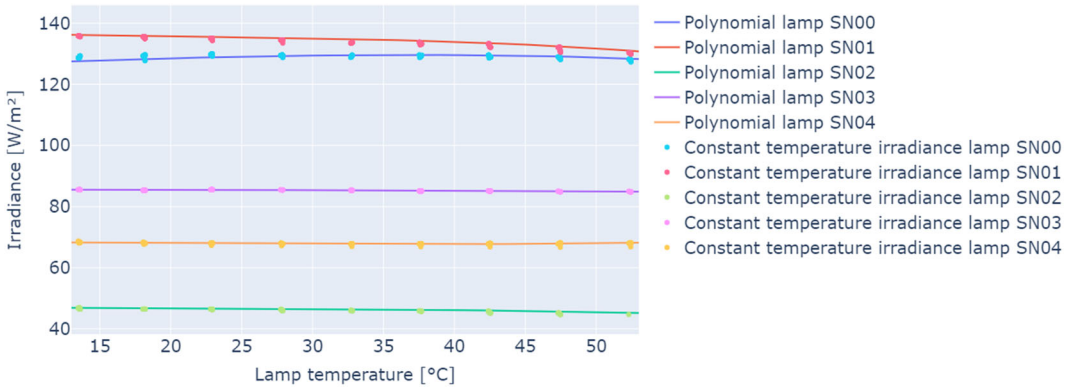

FIGURE 7 Irradiance measurements at several different LED temperatures for several lamps and polynomials used to derive the temperature correction [Colour figure can be viewed at wileyonlinelibrary.com]

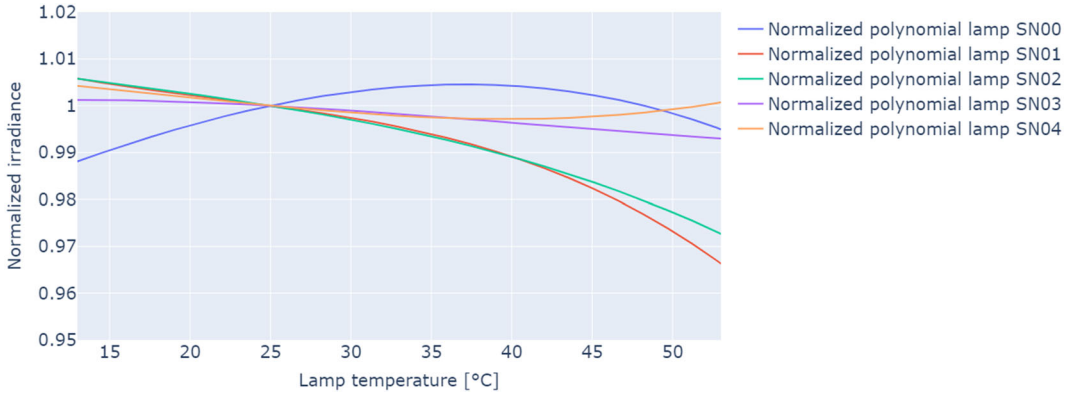

FIGURE 8 Temperature correction factors for several lamps [Colour figure can be viewed at wileyonlinelibrary.com]

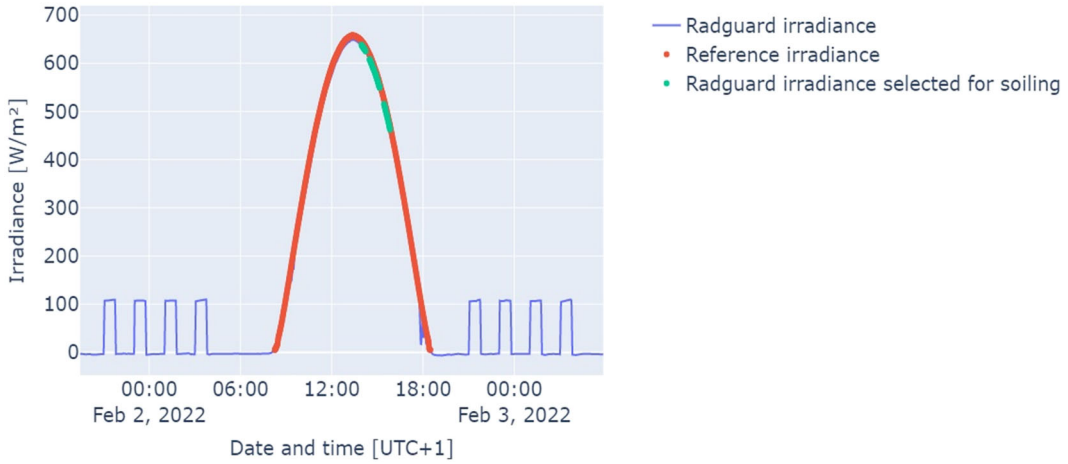

FIGURE 9 Exemplary measurements of the uncleaned test pyranometer (blue) and the reference pyranometer (red) at CIEMAT's PSA. Measurements of the test pyranometer that were used to derive the soiling loss by comparing the irradiance to the reference are shown in green. [Colour figure can be viewed at wileyonlinelibrary.com]

2022 were taken. We start with the presentation of the results for the pyranometer system and continue with those for the reference cell setup.

4.1 | Evaluation of soiling losses of the tested system

During the night, the soiling measurement can be repeated several times. In the beginning of the system test phase beginning 27 December 2021 until 31 January 2022, only one measurement per night was obtained. Since 31 January 2022, four soiling measurements are performed (Figure 9). The more measurements are carried out, the more energy is needed, which might be limited by the capacity of the battery system. On the other hand, the accuracy and quality of the soiling measurements and the statistics increase with the number of measurements each night.

For the first data selection, all signals from a night are evaluated as described in Section 2. Signals collected while the pyranometer was wet or covered with snow or ice are automatically excluded. These data, which is affected by dew or raindrops, are found to be characterized by a high variation of the measured soiling losses during one night.

Another similar source of error can be strong deviations of the visibility at the time of the measurement from that of the night of the calibration of the lamp when $I_{cor,clean}$ was derived. If the visibility during the calibration night and the measurement is different, the radiation extinction between lamp and radiometer is different and Radguard will erroneously interpret the corresponding change of the received irradiance as a soiling effect (soiling or cleaning). The effect is small for most cases but relevant for fog and during sandstorms. Measurements affected by this effect might also be excluded by comparison of the several Radguard measurements during the same night as mentioned above.

The variation of external light during the nightly measurements can also cause errors. The measurements of the parameters O_1 and O_2 before and after the lamp is switched on are used to remove constant background light. High variations of O_1 and O_2 during one measurement (10% deviation) are used to exclude some measurements with variations of the background light. If the background light is only changing while the lamp is switched on so that O_1 and O_2 are the same, the variation will indeed lead to errors.

Afterwards, the mean of the soiling loss measurements and their standard deviation are calculated. Measurements greater or less than the median plus or minus the standard deviation, respectively, are excluded, and the resulting soiling loss is the average of the remaining values. The irradiance measurement of the test pyranometer during a night affected by rain can be seen in Figure 10.

4.2 | Description of the method to derive the reference soiling losses

The calculation of the reference soiling losses involves the comparison of the test radiometer which is illuminated by the lamp to a radiometer of the same model that is cleaned week-daily, so that a soiling loss of 0% can be assumed for this reference radiometer.

To derive the reference soiling loss of the pyranometer, only irradiance data with GHI of more than 400 W/m^2 and direct normal irradiance of more than 600 W/m^2 have been selected, and a quality control was applied on both irradiance signals.[19] Furthermore, only data with direct normal irradiance changes of less than 2 W/m^2 per minute were used. For the reference cell, the filters were adapted to use only GTI data with more than 400 W/m^2 and a change of less than 2 W/m^2 per minute. With these conditions, irregular data are excluded and therefore on days without stable, sunny conditions, no reference soiling losses are derived. Finally, the ratio of the test to the clean radiometer signal was calculated, and outliers with more than 30% deviations were filtered out since this is most likely caused by external shadowing in the data set. The minimum amount of datapoints to calculate the soiling for the day is set to 20. By this, measurements on days with instable conditions are typically not considered, and extreme soiling loss results caused by a small number of unreliable datapoints are avoided. This outlier filter only affects the

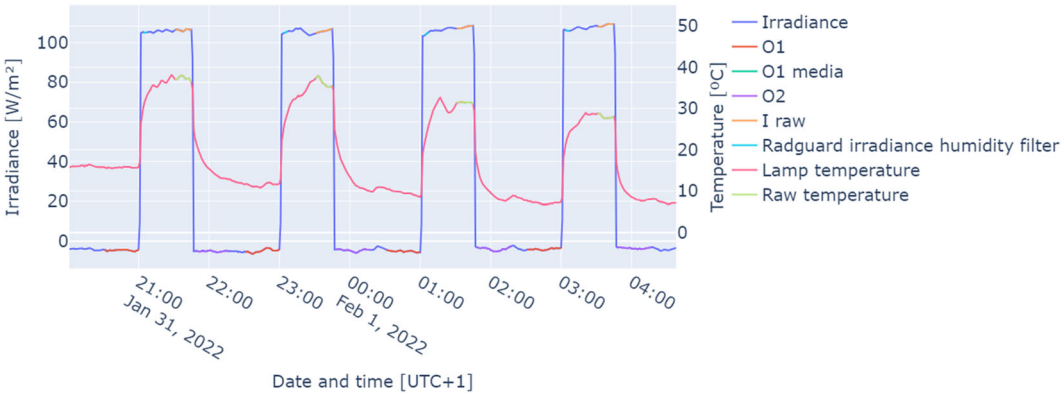

FIGURE 10 Irradiance and temperature of the test pyranometer at night. The four signals measured during night can be different due to dew, rain drops, snow, or frost [Colour figure can be viewed at wileyonlinelibrary.com]

reference data, since the irradiance by the lamp during the night is not affected by the cloud conditions.

In order to avoid an influence to the reference soiling loss measurement by an absolute calibration error, the test and reference radiometers are calibrated relative to each other. During days on which the test and the reference radiometers are both cleaned, the calibration factor c_{rel} is calculated. $c_{rel}(a_i, e_i)$ is derived as the median of the ratios of the test and reference irradiances I_{test} and I_{ref} for solar azimuth and elevation bins a_i and e_j. By this calibration, the slightly different leveling of the two sensors is automatically corrected. The bin sizes are 5° both for solar azimuth and elevation in the case of the pyranometer and 5° for solar azimuth and 10° for solar elevation in the case of the reference cell.

Once calculated, the calibration factors are used for their corresponding solar elevation and azimuth bins to derive the reference soiling losses. For each minute, $S_{ref,min}$ is calculated as

$$S_{ref,min}(\%) = \left(1 - \frac{I_{test}}{I_{ref} \cdot c_{rel}(a_i,\ e_j)}\right) \cdot 100. \quad (5)$$

The median of all $S_{ref,min}$ is then compared to the soiling loss derived by the new Radguard soiling measurement system.

4.3 | Considerations of system changes during the validation campaign

During the test period, several recalibrations are automatically carried out based on a simple logbook in which cleaning, leveling of the radiometers, and repositioning of the lamp are documented.

The days when the test radiometer was cleaned are assumed to have a soiling loss of 0%. Thus, we calculate the calibration factor. In addition, the irradiance of the night after the cleaning event is taken to derive the irradiance $I_{cor,clean}$ from Equation 2 that characterizes the lamp in its current position relative to the radiometer and the clean test radiometer. For the start of the soiling measurements, a clean sensor is indispensable. As the test radiometer has to be cleaned from time to time anyways, the Radguard setup does not require a long-term stable lamp and radiometer, and stability of the lamp and the radiometer is only required for several weeks or few months.

On days when the radiometer was leveled or manipulated but not cleaned, or when the radiometer and the lamp are changed at the same day, the relative calibration factor must be recalculated for obtaining the reference soiling loss considering the reference signal and, in addition, $I_{cor,clean}$ at night must also be updated. Since the radiometer was not cleaned, the $I_{cor,clean}$ cannot be measured directly but must be calculated with the previous soiling loss and the measured irradiance from this night. For this purpose, the reference soiling loss measured on the closest previous valid day is used to increase the measured test irradiance from this night to the irradiance expected with a clean radiometer. If there is no valid soiling loss data from the reference sensor soiling calculation from one of the four previous days, we assume that the soiling conditions are not comparable. In this case, the Radguard soiling loss during the last valid night, considering the last four nights, is taken instead. If it rains after leveling on the same day, the new calculation will not be performed and there will be no new reference irradiance and calibration factor until the radiometer is cleaned again.

When only the lamp is adjusted, the irradiance received during the day is not affected, but the irradiance measured during the night is. In this case, $I_{cor,clean}$ must also be calculated by increasing the nightly irradiance measurement after the change according to the expected soiling loss. The expected soiling loss is the next valid soiling loss from the reference sensor in the four following days after the change. If the soiling loss cannot be calculated because of bad ambient conditions, the expected soiling loss is taken from the last valid Radguard calculation, considering the last four nights before the change.

Figure 11 shows an example on how the nightly irradiance changes due to system changes and soiling. On 27 December 2021, the test system started to measure, being cleaned the first day. For this night, $I_{cor,clean}$ was calculated for the first time, shown as the green line. On 15 January, the test pyranometer was cleaned again, so a new $I_{cor,clean}$ was calculated as indicated in the graph as a change in

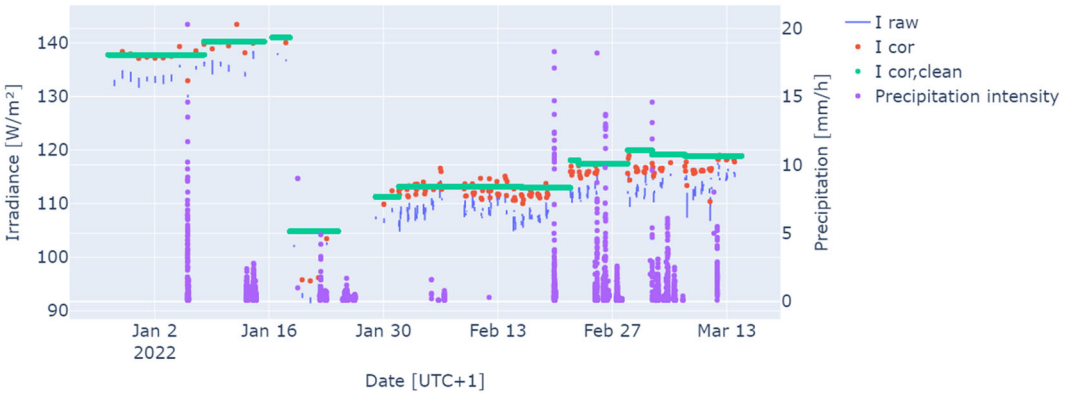

FIGURE 11 Irradiance measurements used for the Radguard soiling measurements. Different irradiance $I_{cor,clean}$ for a pyranometer caused by the lamp due to readjustments of the lamp or pyranometer position. Precipitation data are only shown during precipitation. [Colour figure can be viewed at wileyonlinelibrary.com]

the green line. On 18 January, the lamp was adjusted, and the pyranometer was cleaned. After artificially soiling the pyranometer on January 19, the pyranometer was cleaned again on 24 January. The system was disconnected during several days due to changes of the logger program and working again on 28 January. That day the pyranometer was also leveled, so a new $I_{cor,clean}$ is shown. It was leveled again on 15 and 22 February and on 3 March.

For the reference cell system, the evaluation is less complex as less changes were made to the orientation of both lamp and the cell (see Figure 12). The first calibration was on 18 May due to the start of the soiling analysis. The first change for the $I_{cor,clean}$ on 25 May is caused by an adjustment of the power supply. Due to two cleaning events, with following artificial soiling experiments, the $I_{cor,clean}$ was changed again on 7 and 21 June.

5 | RESULTS OF THE SYSTEM VALIDATION

In this section, the results of the Radguard validation are shown for the two pyranometer setups and the reference cell. We start with the pyranometer validation and continue with the reference cell setup. In order to cover a wide range of soiling levels with the data set, we applied artificial soiling and cleaning at times as described below. For the artificial soiling, fine local soil was distributed on the sensor surface by hand. The sensor was moistened before so that the dust settled on the surface more efficiently. The daily averages of the reference soiling loss are compared to the averages of the nightly soiling loss measurements from the nights before and after the day. This way, the effect of changing soiling losses during the measurement day on the comparison is limited. If the soiling measurement was only possible in one night due to rain, dew, or other reasons, the remaining soiling loss measurement is compared to the reference soiling loss. In order to avoid the influence of natural or manual cleaning on the comparison, data points are not compared to each other if it rained between the test and reference soiling measurements or if the test radiometer was cleaned between them.

5.1 | System validation for the pyranometer

The soiling loss of the test pyranometer is shown in Figure 13 as a function of time. Both the results of the new Radguard method and the reference are presented.

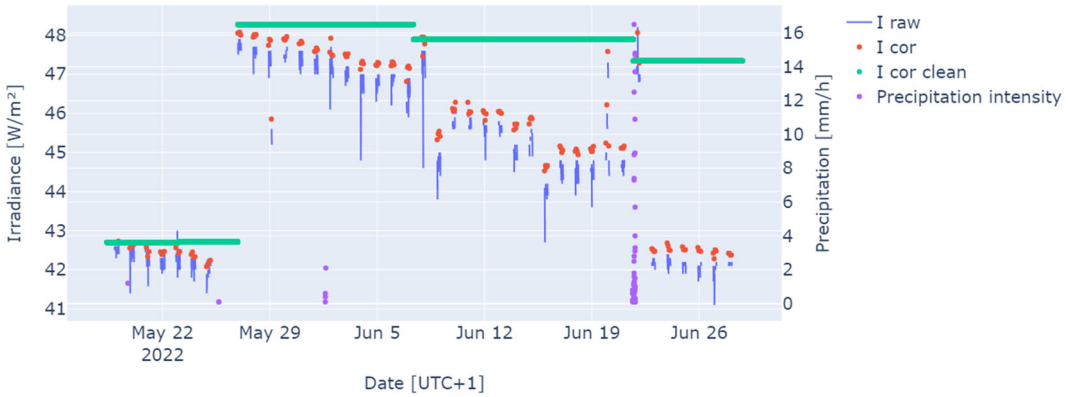

FIGURE 12 Irradiance measurements used for the Radguard PV soiling measurements. The different irradiance $I_{cor,clean}$ for the reference cell is caused by readjustments of the lamp or pyranometer position. Precipitation data are only shown during precipitation. [Colour figure can be viewed at wileyonlinelibrary.com]

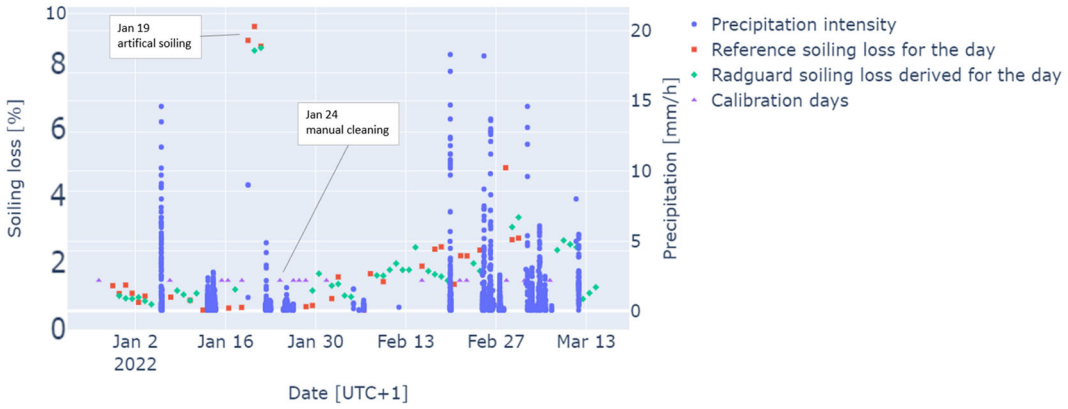

FIGURE 13 Exemplary results of the soiling loss measurement of the new method compared to the reference for a pyranometer installed on a fixed structure at CIEMAT's PSA [Colour figure can be viewed at wileyonlinelibrary.com]

During the first days, low or moderate soiling losses below 1% are found. On 19 January, the pyranometer was artificially soiled as shown in Figure 14. The resulting soiling pattern roughly represents cases that have been observed after the Sahara dust events followed by rain. Despite the visible inhomogeneity of the soiling pattern, the reference and test soiling losses coincide within 0.86% for the affected measurement days. Precipitation cleaned the pyranometer on 22 January, and it was manually cleaned on the 24th to start a new natural soiling interval. From 31 January onwards, the system measures four times each night instead of one time. Rain cleaned the pyranometer again on 19 February, from 25 to 28 February, from 3 to 7 March and on 11 March.

FIGURE 14 Pyranometer dome after artificial soiling on 19 January [Colour figure can be viewed at wileyonlinelibrary.com]

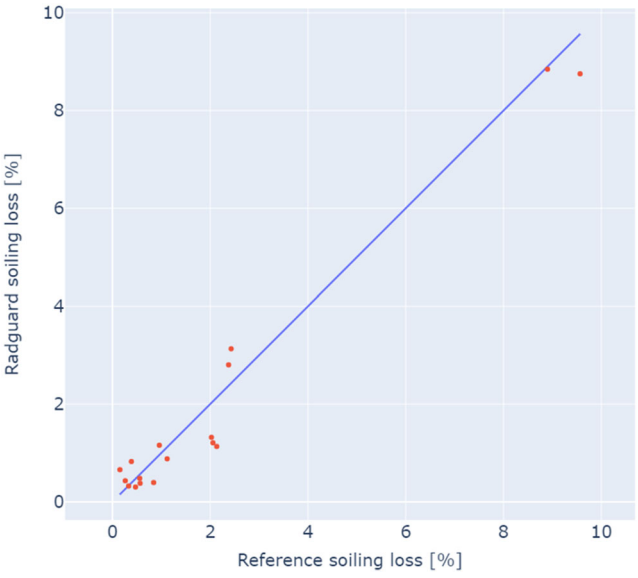

FIGURE 15 Scatterplot of the soiling loss measurement of the new method and the reference for a pyranometer at CIEMAT's PSA [Colour figure can be viewed at wileyonlinelibrary.com]

Figure 15 shows the soiling loss measured from the new system, compared to the reference soiling loss derived from the pair of pyranometers. Most of the points are close to the origin, corresponding to natural soiling, below 3% soiling loss. Points with 8% to 9% soiling loss in the right part of the graph correspond to the soiling experiment carried out in January. The deviations can be characterized by a root mean square deviation of 0.50%, mean absolute deviation of 0.41%, and a bias of −0.12% which is below the expected uncertainties of the reference and the tested method.

5.2 | System validation for the reference cell setup and PV soiling

The soiling loss of the reference cell is shown in Figure 16, where results of the Radguard method and the reference are presented as a function of time. The incidence angle correction described in section 2 has already been applied on the Radguard data. As in the case of the pyranometer system, daily averages of the reference soiling loss are compared to the averages of the nightly soiling loss measurements from the data before and after the day. Again, data points are not compared to each other if it rained between the test and reference soiling measurements or if the test radiometer was cleaned between them.

The measurements started operating on 18 May, being cleaned and calibrated for the first time. During this period the reference cell was only affected by natural soiling, reaching values around 1% soiling loss. On the 1 and 21 June, it rained. On 8, 15, and 22 June, artificial soiling experiments were carried out (Figure 17). Due to unstable ambient conditions during the day, a daily reference soiling loss calculation between the 12 and 22 June was not possible. The program automatically excluded these days for the further calculation due to the small amount of datapoints or a GTI of less than 400 W/m^2, as already described in Section 4.2. During the night, the calculation was still possible because the method is more independent of the ambient conditions than the method during the day.

Figure 18 shows the validation of the soiling loss measurements for the reference cell setup. On the left part, with a soiling loss between 0% and 1%, measurements under natural soiling loss conditions are plotted. These measurements correspond to May and early June. Soiling losses between 2% and 3% correspond to the first artificial soiling experiment carried out between 9 and 12 June. On June 16, after applying the second artificial soiling, 4% soiling loss was obtained. The data with 7% soiling loss correspond to the last soiling experiment. Part of the observed deviations can be explained by the fact that the AOI correction is applied always in the same way for the target AOI of 28° without an adaptation to the actual AOI present during the specific reference measurement. The effect of this simplification is considered to be small compared to the uncertainties of both measurement methods. For higher soiling losses, slightly higher losses are measured by Radguard, but the bias is low with 0.28%. The root

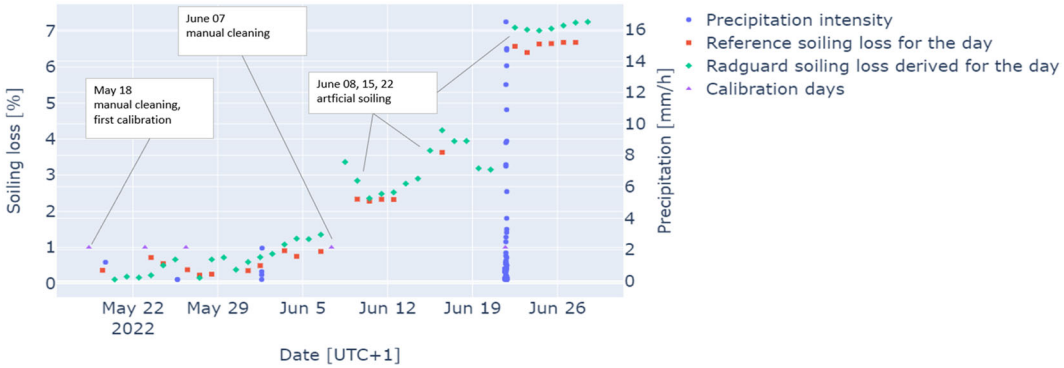

FIGURE 16 Exemplary results of the soiling loss measurement of the new method compared to the reference for a reference cell at CIEMAT's PSA. The angle of incidence correction is applied already. [Colour figure can be viewed at wileyonlinelibrary.com]

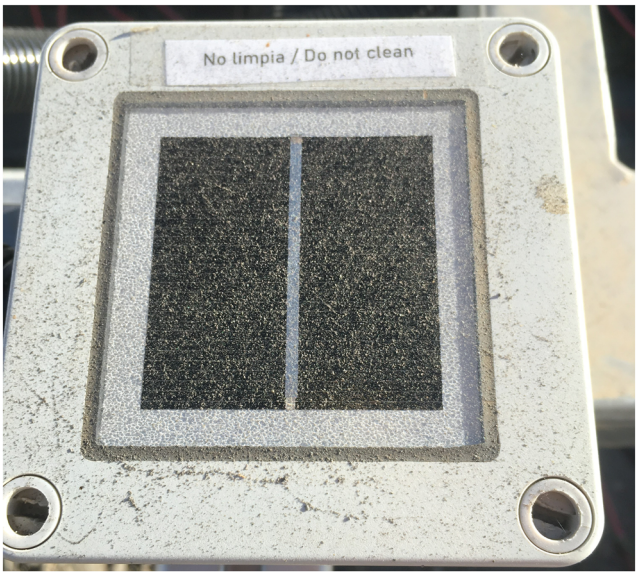

FIGURE 17 Soiled reference cell on 8 June 2022 [Colour figure can be viewed at wileyonlinelibrary.com]

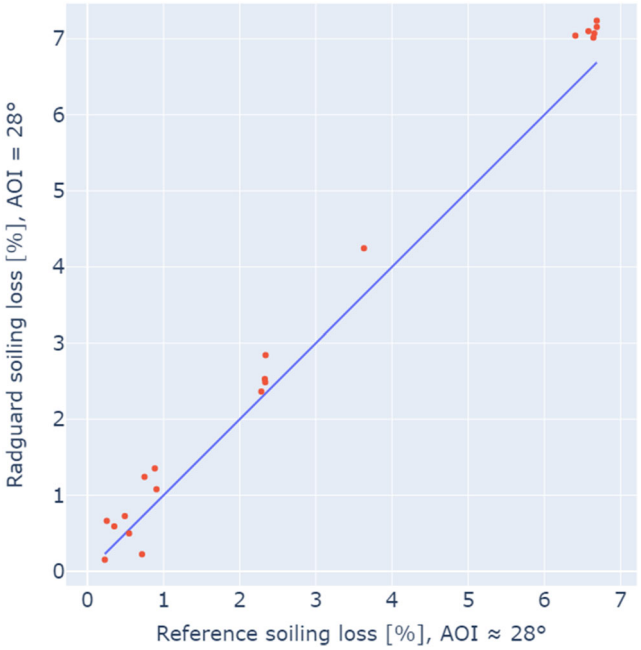

FIGURE 18 Scatterplot of the soiling loss measurement of the new method compared to the reference for a reference cell at CIEMAT's PSA (AOI correction included) [Colour figure can be viewed at wileyonlinelibrary.com]

mean square deviation of the compared data is 0.40%, and the mean absolute deviation is 0.35%. This is below the expected uncertainties of the reference and the tested method.

6 | CONCLUSION

A new measurement method for PV, reference cell, and pyranometer soiling has been developed and validated with 4 months of data from southern Spain. The method uses a lamp that is switched on one or more times for about 45 min at night, and the nightly irradiances are compared to signals from a night with a clean sensor. This method requires low maintenance as the lamp is protected from soiling by a 25-cm-long collimator. Five lamps were characterized in a climate chamber, and temperature corrections for their irradiances were derived. With the currently used lamp model, a temperature correction should be derived individually for each lamp as the corrections are different from each other. Two lamps were installed with a pyranometer and a reference cell for an outdoor test. The measured soiling losses were compared to soiling losses derived by comparing the test radiometer to a clean device of the same model. The deviations between the data sets were found to be below the expected uncertainty of the reference data with low biases of <0.3%.

It was observed that dew or raindrops on the test radiometer can cause erroneous soiling loss measurements and the comparison of four soiling losses each night helped to reduce such errors. For the comparison to the reference soiling losses, rain events were considered to avoid comparing data obtained at night after a natural cleaning event to the soiling losses measured during the day before the rain. This is also recommended for the application of the data in a solar

power plant and for solar radiation measurements. Precipitation measurements or modeled rain data to complement the soiling measurements are hence of interest. The incidence angle correction of the data is considered important for the reference cell setup and implemented for the geometry used in the validation. Such a correction is also of interest for other soiling sensors such as indirect soiling sensors. For the pyranometer, an incidence angle correction was not applied as the geometry of the pyranometer's dome avoids the incidence angle effect.

Studies of the stability of the lamp over several days, weeks, or month are only included indirectly in this work by the comparison of the soiling loss measurement to the reference method. Such stability changes are possible as LEDs are known to change with operating hours and cycles. The presented field calibration method is designed to remove the effect of long-term changes, but changes between two lamp field calibrations are relevant for the measurement accuracy. With the current data, we assume that the lamp is sufficiently stable to provide the observed accuracy if a recalibration of lamp (nightly measurement with clean radiometer) occurs every 2 weeks or more often. Longer intervals between the cleaning events of, for example, 1 or 2 months could be possible, but more detailed studies covering also a longer duration are needed which are the topic of ongoing experiments.

To further improve the Radguard system also other effects caused by the optical characteristics of the lamp might be considered. The LED spectrum is different from the solar spectrum, and the soiling loss depends on the wavelengths.[20] We consider the effect to be smaller than other sources of errors and uncertainty discussed above. The spatial inhomogeneity of the illumination of the radiometer might be another source of errors that can lead to noticeable deviations for inhomogeneous soiling patterns on the radiometer.

In the future, the method will be tested at further sites and in longer measurement campaigns that are now under preparation. The found deviations are seen as a successful validation of the method, in particular considering that a simple pocket light was used as the light source. A promising new soiling measurement method has been developed.

ACKNOWLEDGEMENTS

Open Access funding enabled and organized by Projekt DEAL.

CONFLICT OF INTEREST

The authors declare that they have no known competing financial interests or personal relationships that could have caused a conflict of interest related to the work reported in this paper.

DATA AVAILABILITY STATEMENT

The data that support the findings of this study are available on request from the corresponding author. The data are not publicly available due to privacy or ethical restrictions.

ORCID

José Carballo https://orcid.org/0000-0003-0529-5672

REFERENCES

1. Ilse K, Micheli L, Figgis BW, et al. Techno-economic assessment of soiling losses and mitigation strategies for solar power generation. *Joule*. 2019;3(10):2303-2321. doi:10.1016/j.joule.2019.08.019
2. Geuder N, Quaschning V. Soiling of irradiation sensors and methods for soiling correction. *Sol Energy*. 2006;80(11):1402-1409. doi:10.1016/j.solener.2006.06.001
3. Maxwell EL, Wilcox SM, Cornwall C, et al. *Progress Report for Annex II—Assessment of Solar Radiation Resources in Saudi Arabia 1993-1997, NREL/TP-560-25374*. National Renewable Energy Laboratory; 1999.
4. Forstinger A, Wilbert S, Driesse A, Kraas B. Uncertainty calculation method for photodiode pyranometers. *Solar RRL*. 2022;6(5):2100468. doi:10.1002/solr.202100468
5. Cristaldi L, Faifer M, Rossi M, et al. Economical evaluation of PV system losses due to the dust and pollution. In: *2012 IEEE International Instrumentation and Measurement Technology Conference Proceedings*. IEEE; 2012.
6. Kagan S, Giosa E, Flottemesch R, et al. Impact of non-uniform soiling on pv system performance and soiling measurement. In: *2018 IEEE 7th World Conference on Photovoltaic Energy Conversion (WCPEC) (A Joint Conference of 45th IEEE PVSC, 28th PVSEC & 34th EU PVSEC)*. IEEE; 2018.
7. Wolfertstetter F, Esquelli A, Wilbert S, et al. Incidence angle and diffuse radiation adaptation of soiling ratio measurements of indirect optical soiling sensors. *J Renew Sustain Energy*. 2021;13(3):033703. doi:10.1063/5.0048001
8. Gostein M, Caron JR, Littmann B. Measuring soiling losses at utility-scale PV power plants. In: *2014 IEEE 40th Photovoltaic Specialist Conference (PVSC)*. IEEE; 2014.
9. Korevaar M, Mes J, Nepal P, Snijders G, van Mechelen X. Novel soiling detection system for solar panels. *Paper presented at: 33rd European Photovoltaic Solar Energy Conference and Exhibition*; September 25-29, 2017; Amsterdam, Netherlands. doi:10.4229/EUPVSEC20172017-6BV.2.11
10. Gostein M, Faullin S, Miller K, Schneider J, Stueve B. Mars Soiling Sensor™. In: *2018 IEEE 7th World Conference on Photovoltaic Energy Conversion (WCPEC) (A Joint Conference of 45th IEEE PVSC, 28th PVSEC & 34th EU PVSEC)*. IEEE; 2018.
11. Morley K, Robinson J, Chard J, Peterson J. In-situ comparison of five soiling measurement systems. In: *PVPMC Webinar on Solar Resource Assessment*. August 5 2020; New Mexico, CA and Utah.
12. Borg E, Schmidt K, Renke F, Spengler D. Vefahren zum Schätzen eines Zustandes eines Globalstrahlungssensors und Messstation mit Globalstrahlungssensor; 2018.
13. Fernández-Solas Á, Micheli L, Muller M, Almonacid F, Fernández EF. Design, characterization and indoor validation of the optical soiling detector "DUSST". *Sol Energy*. 2020;211:1459-1468. doi:10.1016/j.solener.2020.10.028
14. Micheli L, Morse J, Fernandez EF, Almonacid F, Muller M. *Design and Indoor Validation of 'DUSST': A Novel Low-Maintenance Soiling Station*. National Renewable Energy Laboratory; 2018.
15. Muller M, Micheli L, Solas AF, et al. An in-depth field validation of "DUSST": a novel low-maintenance soiling measurement device. *Prog Photovolt: Res Appl*. 2021;29(8):953-967. doi:10.1002/pip.3415
16. John J, Rajasekar V, Boppana S, Tatapudi S, Tamizhmani G. Angle of incidence effects on soiled PV modules. In: *Reliability of Photovoltaic Cells, Modules, Components, and Systems VII*. SPIE; 2014.
17. Martin N, Ruiz J. A new model for PV modules angular losses under field conditions. *Int J Sol Energy*. 2002;22(1):19-31. doi:10.1080/01425910212852
18. Zorrilla-Casanova J, Philiougine M, Carretero J, et al. Analysis of dust losses in photovoltaic modules. In: *World Renewable Energy Congress-Sweden*. Linköping University Electronic Press; 2011.

19. Geuder N, Wolfertstetter F, Wilbert S, et al. Screening and flagging of solar irradiation and ancillary meteorological data. *Energy Procedia*. 2015;69:1989-1998. doi:10.1016/j.egypro.2015.03.205
20. Micheli L, Caballero JA, Fernandez EF, et al. Correlating photovoltaic soiling losses to waveband and single-value transmittance measurements. *Energy*. 2019;180:376-386. doi:10.1016/j.energy.2019.05.097

How to cite this article: Campos L, Wilbert S, Carballo J, et al. Autonomous measurement system for photovoltaic and radiometer soiling losses. *Prog Photovolt Res Appl*. 2022;1-14. doi:10.1002/pip.3650